PCCP

Accepted Manuscript

This is an *Accepted Manuscript*, which has been through the Royal Society of Chemistry peer review process and has been accepted for publication.

Accepted Manuscripts are published online shortly after acceptance, before technical editing, formatting and proof reading. Using this free service, authors can make their results available to the community, in citable form, before we publish the edited article. We will replace this *Accepted Manuscript* with the edited and formatted *Advance Article* as soon as it is available.

You can find more information about *Accepted Manuscripts* in the Information for Authors.

Please note that technical editing may introduce minor changes to the text and/or graphics, which may alter content. The journal's standard Terms & Conditions and the Ethical guidelines still apply. In no event shall the Royal Society of Chemistry be held responsible for any errors or omissions in this *Accepted Manuscript* or any consequences arising from the use of any information it contains.

ROYAL SOCIETY OF CHEMISTRY

www.rsc.org/pccp

Journal Name
Physical Chemistry Chemical Physics
Dynamic Article Links ►
Cite this: DOI: 10.1039/c0xx00000x
www.rsc.org/xxxxxx
ARTICLE TYPE

Extreme strain rate and temperature dependence of mechanical properties of nano silicon nitride thin layer in basal plane under tension: a molecular dynamics research

Xuefeng Lu,[a] Hongjie Wang,*[a] Yin Wei,[a] Jiangbo Wen,[a] Min Niu[a] and Shuhai Jia*[b]

Received (in XXX, XXX) Xth XXXXXXXXX 20XX, Accepted Xth XXXXXXXXX 20XX
DOI: 10.1039/b000000x

Molecular dynamics simulations are performed to clarify the extreme strain rate and temperature dependence of mechanical behaviors of nano silicon nitride thin layer in basal plane under tension. It is found that fracture stresses almost no change with increasing strain rate. However, fracture strains decrease gradually due to the appearance of additional N^{2c}-Si bonds breaking defects in the deformation process. With increasing loading temperature, there is a noticeable drop in fracture stress and fracture strain. In the low temperature range, the roughness phases can be observed owing to a combination of factors that configuration evolution and energy change.

1 Introduction

The effort for hunting the materials with outstanding structural stability and remarkable mechanical properties is a task of scientific and technological interest. Recent achievements in nanomechanical experiments are demonstrating superior mechanical properties of nanosized ceramics and wishers, which are distinct from their bulk counterparts.[1-3] Stirred by the surge and the discovery of the superelastic and spring properties of Si_3N_4 microcoils,[4-5] the synthesis of silicon nitride in nanoscale, such as nanowire,[6] nanorod,[7] and nanobelt,[8] has swallowed great efforts and been a subject in a majority of experimental studies. Simultaneously, considerate sweats have also been devoted to investigate their microscopic properties using first-principles and molecular dynamic (MD) methods with satisfactory results.[9-13] Vashishta investigated dynamic fracture in nanophase Si_3N_4 using 106-atom molecular-dynamics simulation and showed that intercluster regions are amorphous and they deflect cracks and give rise to local crack branching.[14] Ching investigated a model of Y-doped intergranular glassy film in Si_3N_4 ceramics by large-scale ab initio modeling and concluded that this microstructure has a complex nonlinear deformation under stress and Y doping significantly enhances the mechanical properties.[15]

The preparation and comprehension of stimuli-responsive materials are concerned predominantly because they provide a mechanism for designing nanoscale devices and for improving the performance of devices. Moreover, the mechanical control of nanomaterials and nanosystems is emerging as a fascinating means for exploring the unique properties and potential applications of nanoscale materials.[16-18] However, for the mechanical properties of nano β-Si_3N_4 thin layer, the absence of the samples of nano-sized crystals used in experimental measurements with perfect crystal configuration does not currently allow a direct observation of the different mechanical behavior during loading. This encouraged us to explore the novel mechanical responses of β-Si_3N_4 under various conditions in nanometer range. In the previous work, we conducted uniaxial tension of β-Si_3N_4 thin layers in basal plane by atomistic simulations and concluded that the deterioration in mechanical properties derives from the N^{6h}-Si bonds where the fracture is initiated.[19] The objective of current work in this paper is to investigate extreme strain rate and temperature dependence of mechanical properties of nano β-Si_3N_4 thin layer under tension by molecular dynamics. Stress-strain relations are calculated in terms of different tensile strain rates and temperature, and changes in the atomic structure of nano thin layers are analyzed by bonding and structural correlations.

2 Computational details

2.1 The interatomic potential

It is crucial to employ accurate interatomic potentials illustrating a wide range of experimental properties in order to clarify materials' properties and atomic processes quantitatively. From empirical potential models available for covalent systems, the interatomic potential used here in all simulations is the effective potential proposed by Tersoff.[20-21] The potential is based on a proven expression that embodies two- and three-body interactions. The two-body terms are composed of steric repulsion among atoms, a charge-dipole interaction that involves

[a] *State Key Laboratory for Mechanical Behavior of Materials, Xi'an Jiaotong University, Xi'an, 710049, China*
E-mail: hjwang@mail.xjtu.edu.cn; Fax:029-82663453; Tel: 029-82667942
[b] *School of Mechanical Engineering, Xi'an Jiaotong University, Xi'an 710049, China*
E-mail: shjia@mail.xjtu.edu.cn; Fax:029-82668556; Tel: 029-82668556

Physical Chemistry Chemical Physics Accepted Manuscript

the large electronic polarizability of nitrogen, and a screened coulomb interaction owing to charge transfer between Si and N. Three-body interactions consist of covalent effects through bond-bending and bond-stretching terms. This expression has been parameterized and employed successfully to research a wide range of carbides and nitrides.[22-24] In the case of Si_3N_4 studied here in this paper, this robust potential is parameterized to match the bulk modulus and elastic constants of Si_3N_4 to experimental values.

2.2 Simulation setup and details

We carry out MD simulations of a theoretical tensile experiment under different conditions on β-Si_3N_4 thin layers in basal plane, illustrated in Fig.1. β-Si_3N_4, classified as hexagonal, possesses two formula units (14 atoms, as indicated by brown solid line) and can be built as a stacking of the idealized Si-N layer in an ABAB… sequence. All the Si atoms are equivalent (6h sites, light blue atoms), but there are two inequivalent nitrogen sites that N^{2c} atoms (navy blue atoms) in a planar geometry with three nearest Si neighbors and N^{6h} atoms (light green atoms) in slight puckered sites surrounded by three Si atoms, simultaneously, Si atoms are at the center of slightly irregular tetrahedron bonded with one N^{2c} atom and three N^{6h} atoms. The thin layer model is approaching square with the thickness of 0.291 nm and side length of about 15.21 nm. Zigzag and armchair edges are oriented along the x and y directions, respectively. The software package Lammps and visualization program Atomeye are employed for the MD simulation. No periodic boundary conditions are applied. Prior to loading, the initial thin layer configuration structures are fully optimized to an equilibrium minimum energy using the steepest descent algorithm so as to obtain stable configuration and then thermally equilibrated to different temperature using Nose-Hoover thermostat ensemble with a time step of 0.5 fs. After equilibration, the uniaxial tensile loading is applied at both ends with various strain rates in the x direction. The simulated elongation steps are repeated until the thin layers are fully ruptured and well separated.

3 Results and discussion

3.1 Extreme strain rate dependence of Si_3N_4 thin layer

To clarify the strain rate dependence and influence mechanism, we investigate the mechanical behaviors of Si_3N_4 thin layer subjected to uniaxial tension with different extreme strain rates. In this case, the length of the square Si_3N_4 thin layer is around L=152.1 Å in the loading direction. Fig.2 indicates the simulated stress-strain curves for the Si_3N_4 thin layer in zigzag direction. Note that the strain is defined as the percentage of extension of the entire thin layer in the loading direction. The fracture stress is determined as the peak stress and the corresponding strain is the fracture strain. From product data in Fig.2, it is found that the thin layers display nonlinear ($\varepsilon<0.05$), linear response ($0.05<\varepsilon<0.08$), and nonlinear ($\varepsilon>0.08$) stress-strain relationships until fracture occurs. The fracture stresses almost no change accompanying the increasing of strains, illustrating that the strain rate has no obvious effect on the fracture stress. However, the fracture strains decrease gradually from 0.118 to 0.112 when the strain rate increases from 2.6×10^9 to $5.3\times10^9 s^{-1}$. The strain rate dependence of fracture strain can be illustrated in Fig.3 and 4, as follows.

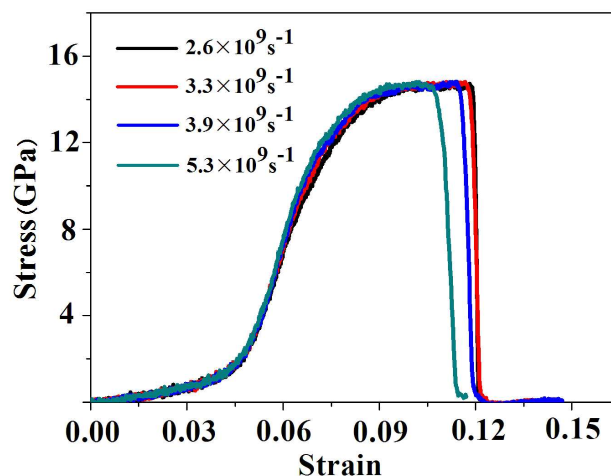

Fig.2 Stress-strain curves of β-Si_3N_4 thin layer under tensile loading with different extreme strain rates in the x (zigzag) direction

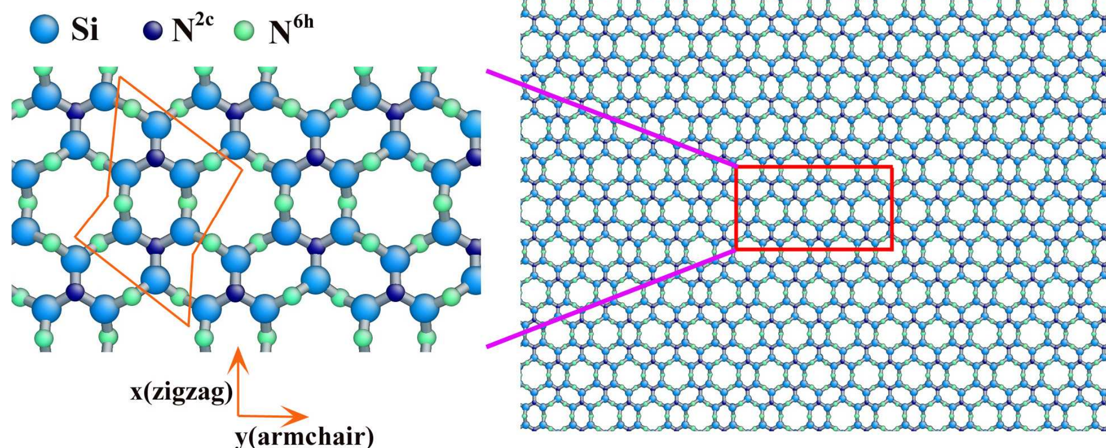

Fig.1 The simulation bonding configuration of β-Si_3N_4 thin layer Si: light blue atoms; N^{2c}: navy blue atoms; N^{6h}: light green atoms

This journal is © The Royal Society of Chemistry [year]
Physical Chemistry Chemical Physics Accepted Manuscript

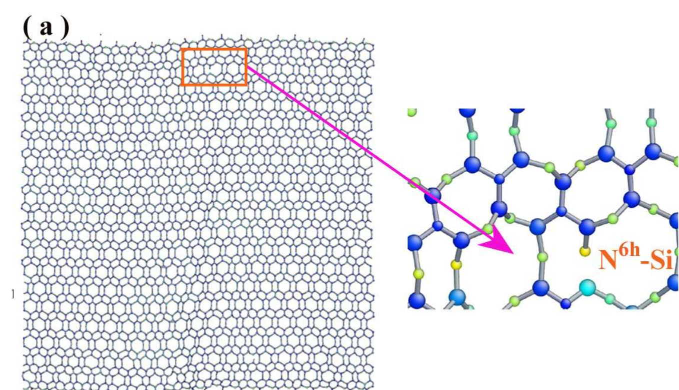

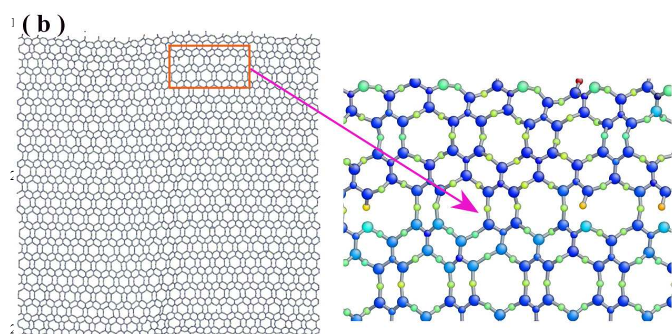

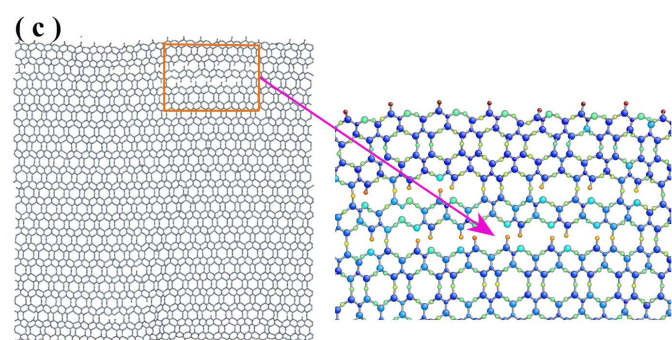

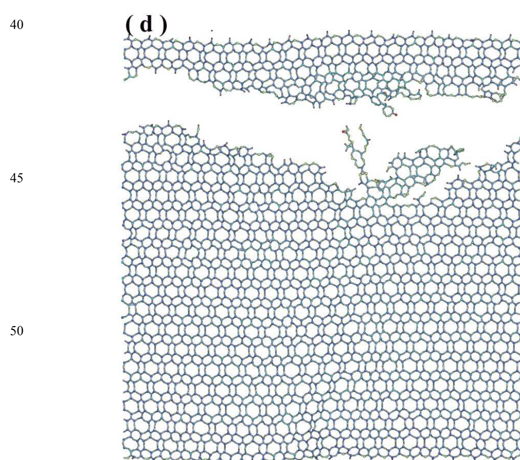

Fig.3 Snaps of β-Si_3N_4 thin layer under tensile loading **with the stain rate of 2.6×10^9** at strains of (a) 0.061, (b) 0.068, (c) 0.080 and (d) 0.121.

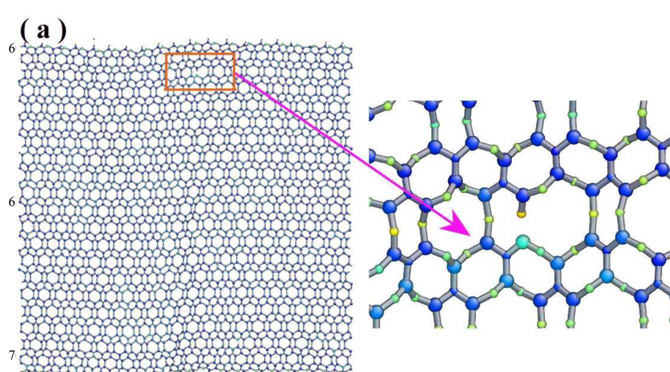

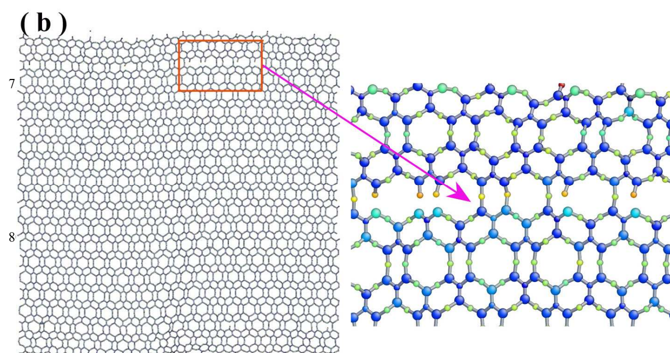

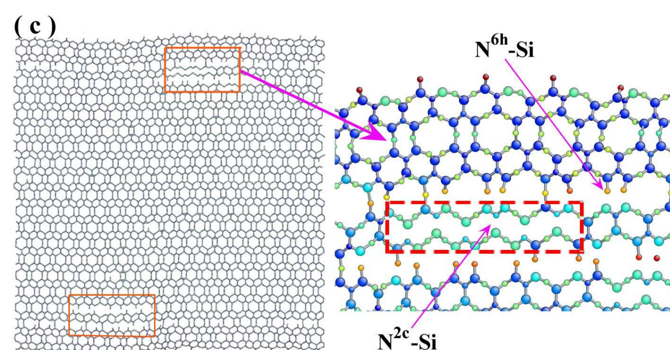

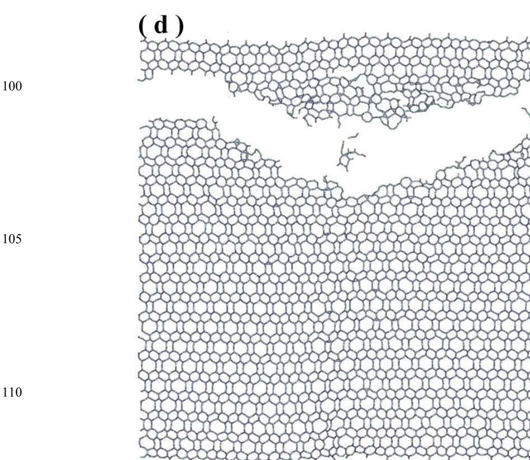

Fig.4 Snaps of β-Si_3N_4 thin layer under tensile loading **with the stain rate of 5.3×10^9** at strains of (a) 0.061, (b) 0.068, (c) 0.080 and (d) 0.113.

Physical Chemistry Chemical Physics Accepted Manuscript

In order to take an insight into the deformation mechanism and fracture details of thin layers responsible for the strain rate dependence and to visualize the process of tensile deformation, we consider the typical snapshots of the atomic arrangements of thin layers with strain rates of 2.6×10^9 and 5.3×10^9 s^{-1}, respectively. For the former at a strain of 0.061 (shown in Fig.3 (a)), the initial N^{6h}-Si bond breaking defect on the top edge of thin layer can be observed as indicated in brown box. Fig.3 (b) displays the evolution configuration at a strain of 0.068. It is clearly found that the number of N^{6h}-Si bond defects comes to three. When the thin layer is elongated to a strain of 0.080 (see Fig.3 (c)), the number of defects distributed in two lines increases to fifteen or so and then the formation and propagation of crack are present, and the thin layer begins to fracture. As the thin layer breaks into two parts completely, the strain comes to 0.121, as illustrated in Fig.3 (d). The above-mentioned analysis shows that the deterioration in mechanical property derives from the N^{6h}-Si bonds where the fracture is initiated and subsequently spreads in all directions. For the latter at strains of 0.061 and 0.068 (indicated in Fig.4 (a) and (b)), the initial bonding breaking defect and evolution configuration are similar with those occurred in the former. When the strain arrives to 0.080 (see Fig.4 (c)), not only N^{6h}-Si but also N^{2c}-Si bonds breaking defects can be observed in the top edge of thin layer, as shown by red dashed box, which contributes to the spread of crack. When the strain rates are in the range of 2.6×10^7 to 2.6×10^{10}, the final fractures all occur in the top of thin layers, similar to that described above. Simultaneously, it is worth noting that the bonds breaking defects are also present in the lower edge. In the course of subsequent fracture, the N^{6h}-Si and N^{2c}-Si bonds breaking defects, acting as a major role, are conductive to the start and rapid expansion of cracks, in combination with the bonds breaking defects located at lower edge, together leading to the appearance of low fracture strain of 0.112. As the evolution of thin layer elongation, the two separated portions can be obtained at a strain of 0.113. Therefore, the extreme strain rate dependence of fracture strain can be attributed to the appearance of the additional N^{2c}-Si bonds breaking defects and the assistant role of defects located at lower edge.

3.2 Temperature dependence of Si_3N_4 thin layer

To further clarify the relationship between the mechanical properties and loading temperature, the mechanical behaviors of Si_3N_4 thin layer under uniaxial tension in zigzag direction with various temperatures are researched and plotted in Fig.5. It can be seen that the stress-strain curves mainly consist of linear and nonlinear phases under the conditions of 100K, 300K and 500K. The fracture stresses, sensitive to the temperature, decrease gradually from 20.4 to 14.3 GPa with increasing loading temperature. When the strains exceed 0.6, 0.8 and 0.9, respectively, the toughness phases can be observed. For the other curves at temperatures of 700K, 900K and 1100K, respectively, the typical nonlinear phases are not present in the stress-strain curves, indicating that thin layers exhibit brittle fracture behaviors in the course of uniaxial tension loading. The fracture stresses drop from 15.3 to 8.6 GPa when the loading temperature increases to 1100K. The results reveal that there is a noticeable drop in both the fracture stress and fracture strain with increasing loading temperature. Simultaneously the roughness phases are present in the temperature range of 100K to 300K and disappear

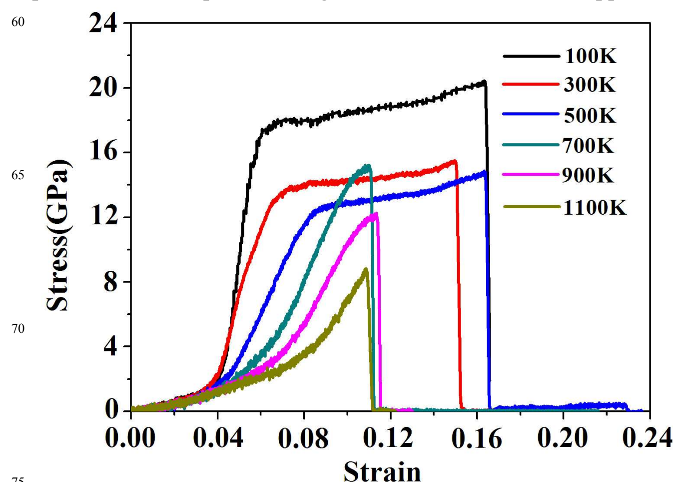

Fig.5 Stress-strain curves of β-Si_3N_4 thin layer under tensile loading with different temperatures in the x (zigzag) direction

in the range of 700K to 1100K, which is maybe attributed to the a combination of factors that configuration evolution and energy change, as described below.

The configuration evolution affects the behavior response mentioned above, and further causing the resulted stress-strain curves. We take representational snapshots of thin layer under tensile loading with different strains at 500K and 700K, respectively, for the purpose of capturing the origin, as shown in Fig.6. It can be seen from Fig.6 (a) and (b) that N^{6h}-Si bonds breaking defects are visible at strains of 0.063 and 0.067, respectively, in the beginning phase of stretch. The number of defects increases by degrees with the elongation of thin layer. When the strain comes to 0.084 (see Fig.6(c)), the number of defects remarkably increases to around 10 at the top edge of thin layer. It is interesting to note that single N atom defect can be seen at the bottom edge of thin layer as the red circle points to. Taken together, the structure of thin layer has almost no change at $\varepsilon<0.090$. However, the configuration deviates from the origin structure as the strain goes into the toughness interval described in Fig.6 (d). Apart from the original N^{6h}-Si bonds breaking defects, the newly emerging Si-Si-N^{2c} bonds breaking defects are visible both at the top edge and middle of thin layer when the strain is 0.101, resulting in the formation of similar layered structure. With the process of tensile loading, other new defects that N^{2c}-Si bonds breaking appear at a strain of 0.122 in Fig.6 (e). The number of N^{2c}-Si bonds breaking rapidly increases and reaches dozens or so, which leads to the formation of complete layered and chain structure at a strain of 0.155 (see Fig.6(f)) as displayed in both the red boxes. When the strain increases to 0.163, the initial crack of thin layer is present shown in Fig.6 (g). With the propagation of crack and energy release, the initial network structure can be achieved again in the area near the crack at a strain of 0.167, as depicted in Fig.6 (h). Finally, the thin layer is divided into two parts demonstrated in Fig.6 (i). Based on the above, the formation of major single N atom, lots of N^{6h}-Si and N^{2c}-Si bonds breaking defects are conductive to the occurrence of roughness phase. On the contrary, the layered and chain

Physical Chemistry Chemical Physics Accepted Manuscript

This journal is © The Royal Society of Chemistry [year]

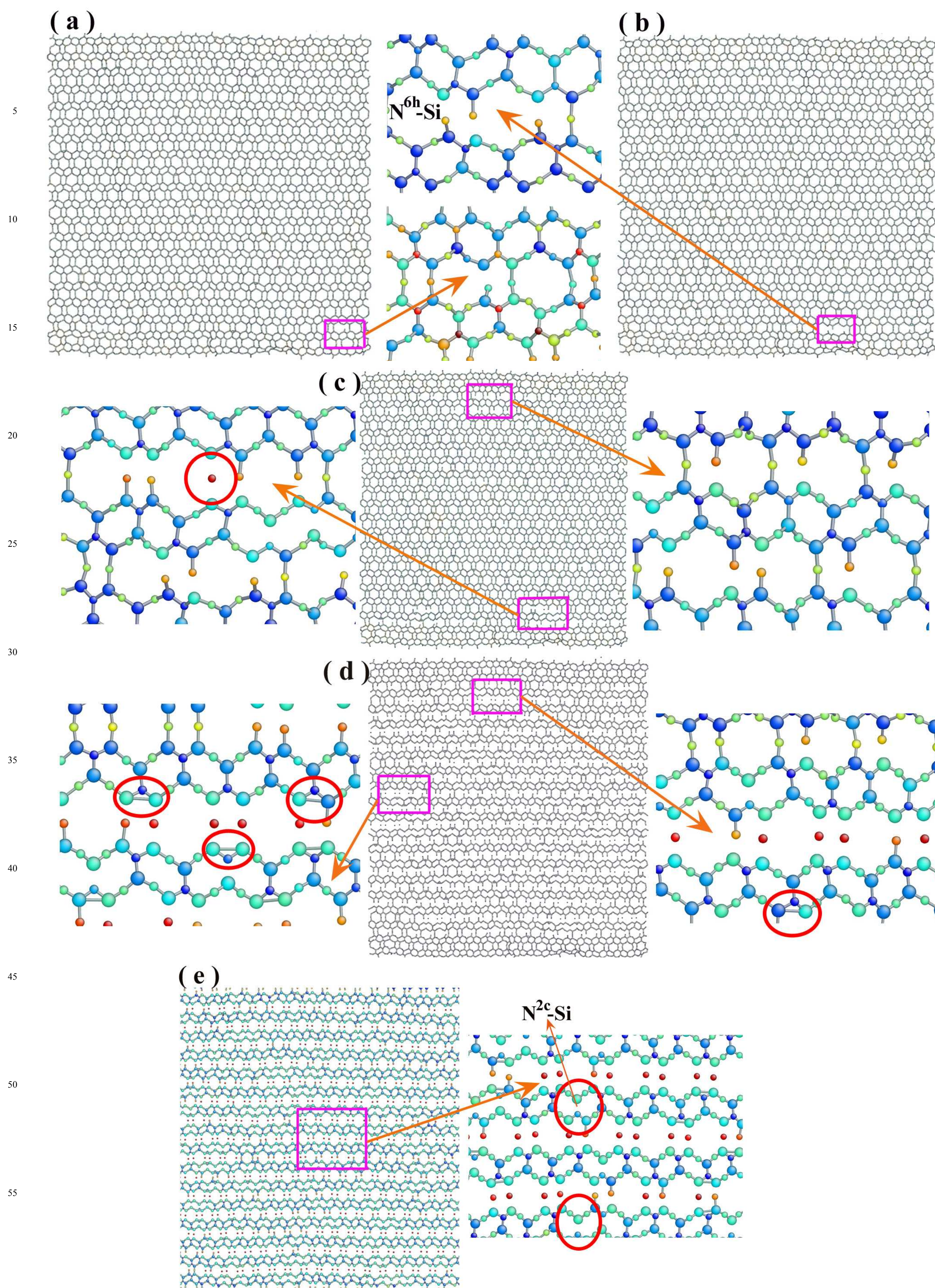

Physical Chemistry Chemical Physics Accepted Manuscript

Fig.6 Snapshots of β-Si_3N_4 thin layer under tensile loading at 500K with strains of (a) 0.063, (b) 0.067, (c) 0.084, (d) 0.101, (e) 0.122, (f) 0.125, (g) 0.163, (h) 0.167 and (i) 0.169

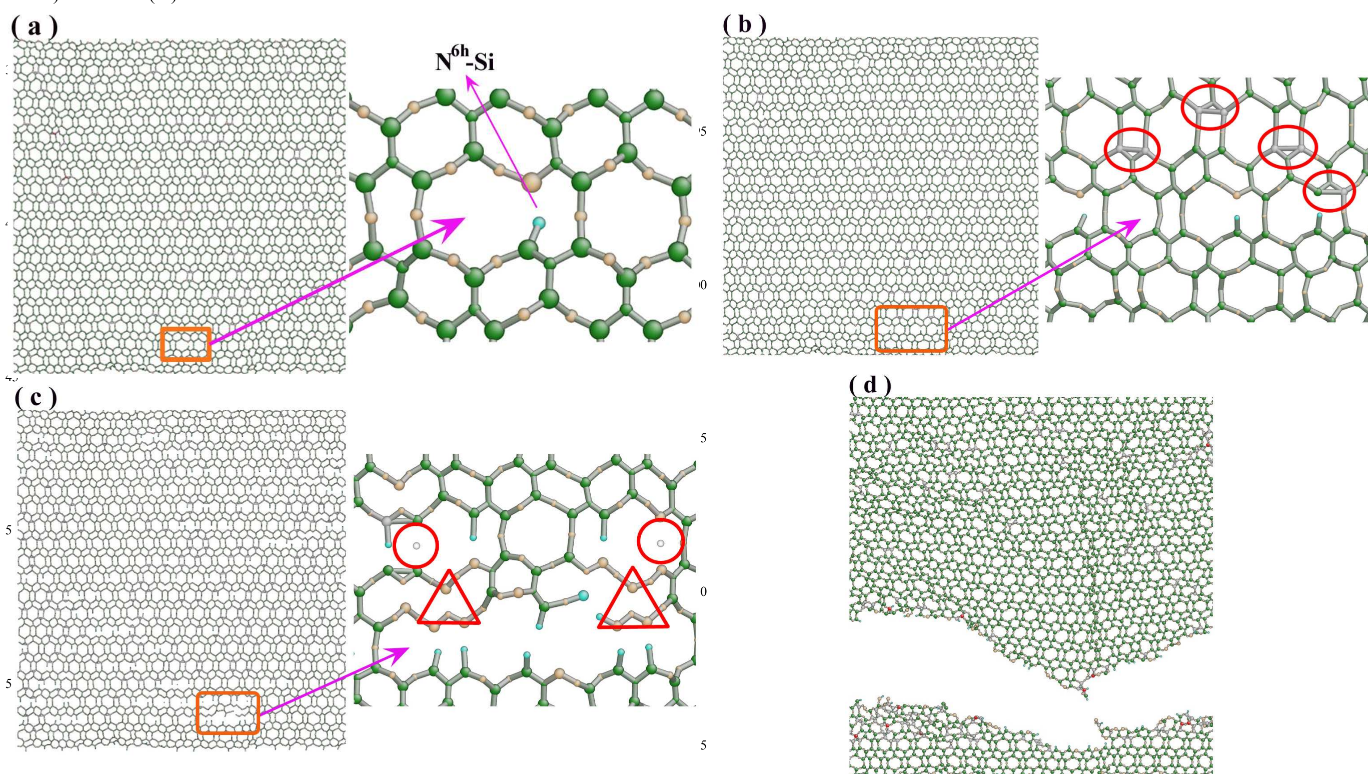

Fig.7 Snapshots of β-Si_3N_4 thin layer under tensile loading at 700K with strains of (a) 0.084, (b) 0.089, (c) 0.102, (d) 0.110

This journal is © The Royal Society of Chemistry [year]

Physical Chemistry Chemical Physics Accepted Manuscript

configuration can not be observed for the thin layer under tensile loading in the snapshots at 700K, as indicated in Fig.7. Similar to the fracture behavior at 500K in the beginning phase, the N^{6h}-Si and Si-Si-N^{2c} bonds breaking and can be seen at strains of 0.084 and 0.089 (see Fig.7 (a) and (b)), respectively, as mentioned above. When the thin layer is stretched to a strain of 0.102, the initial crack occurs. Unlike the previous fracture process, the chain configuration is not present although the presences of individual N atoms and N^{2c}-Si bonds breaking defects, as displayed in Fig.7 (c) by red circles and triangles, causing the brittle fracture behavior of thin layer. The ultimate fracture snapshot is illustrated at a strain of 0.110 in Fig.7 (d). Simultaneously, it is found that the fracture strain is less sensitive to temperature in two ranges that 100-500K and 700-1100K in conjunction with Fig.5.

In addition to the reason of configuration, energy evolution is another factor that is responsible for the fracture behavior. Fig.8 shows the strain-total energy curves for thin layer under tensile loading with various temperatures. It can be clearly seen that total energies firstly increase and then drops with increasing strains. For thin layer at temperatures in the range of 100 to 500K, the maximum values of total energies are about -7.1×10^{-15}J, which are notably higher than that obtained for thin layers at temperatures in the range of 700 to 1100K. Combined with the configuration evolution demonstrated in Fig.7 (e-f), the higher total energies provide the energy required for the formation of major single N atom, lots of N^{6h}-Si and N^{2c}-Si bonds breaking defects, leading to similar layered and chain structure. In which, for the red and light blue of atoms, the corresponding color spectrum representing energy distribution[11,19] also indicates the thin layers exhibit higher energies and larger tensile deformation, which are also in accordance with the results in Fig.5. Relatively speaking, the maximum energies in later three curves are lower and can not meet the requirement for chain structure, resulting in the drop of fracture stress and fracture strain and the disappearance of toughness phase.

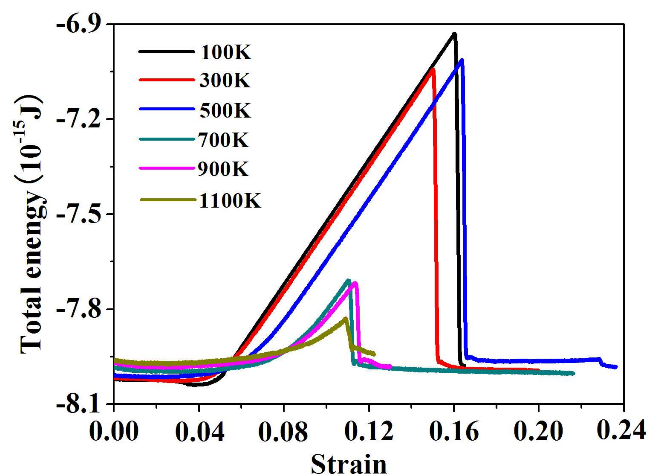

Fig.8 Strain-total energy curves of β-Si_3N_4 thin layer under tensile loading with different temperatures in the x (zigzag) direction

4 Conclusions

In summary, we conduct the study on the extreme strain rate and temperature dependence of mechanical properties of nano silicon nitride thin layer in basal plane under tension by molecular dynamics simulation. The results demonstrate that the fracture strains decrease gradually from 0.118 to 0.112 when the strain rate increases from 2.6×10^9 to $5.3\times10^9 s^{-1}$. Fracture stresses almost no change with increasing strain rate. With increasing loading temperature, there is a noticeable drop in fracture stress and fracture strain. **There are two groups of curves of the temperature dependent stress-strain data, group 100K-500K and group 700-1100K. Consequently, there is a critical temperature point around 600K.** In the low temperature range, the roughness phases can be observed when the strains exceed 0.6, 0.8 and 0.9, respectively. One reason is that the formation of major single N atom, lots of N^{6h}-Si and N^{2c}-Si bonds breaking defects are conductive to the occurrence of roughness phase. Another reason is that higher total energies provide the energy required for the formation of bonds breaking defects, leading to similar layered and chain structure. Thus, configuration and energy evolution are all responsible for the presence of toughness phase. The above results suggest that the nano silicon nitride thin layers are suitable for nanodevices employed in severe environments. Capturing a ceramic with outstanding toughness properties is a dream for ceramic researchers. The insight on the various mechanical behaviors of thin layer is illustriously meaningful and this will be our future research subject.

Acknowledgements

The authors gratefully acknowledge the financial support provided by the National Natural Science Foundation of China (51272206, U1233116), The Ministry of Education Innovation Team Development Plan (IRT1280) and National Key Laboratory Functional Composite (9140C560109130C56201).□

References

1 M. A. Meyers, A. Mishra and D. J. Benson, *Prog. Mater. Sci.,* 2006, **51**, 427-431.

2 K. Momeni and H. Attariani, *Phys. Chem. Chem. Phys.,* 2014, **16**, 4522-4527.

3 J. W. Zhang, C. Jiang, D. Z. Jiang and H. X. Peng, *Phys. Chem. Chem. Phys.,* 2014, **16**, 4378-4385.

4 D. Q. Zhang, A. Alkhateeb, H. Han, H. Mahmood and D. N. Mcllroy, *Nano Lett.,* 2003, **3**, 983-987.

5 C. Cao, H. L. Du, Y. J. Xu, H. S. Zhu, T. H. Zhang and R. Yang, *Adv. Mater.,* 2008, **20**, 1738-1743.

6 W. Q. Han, S. Fan, Q. Li, and B. L. Gu, *Appl. Phys. Lett.,* 1997, **71**, 2271-2274.

7 X. C. Wu, W. H. Song, B. Zhao, W. D. Huang, M. H. Pu, Y. P. Sun, and J. J. Du, *Solid State Commun.,* 2000, **115**, 683-688.

8 K. F. Huo, Y. W. Ma, Y. M. Hu, J. J. Fu, B. Lu, Y. N. Lu, Z. Hu, and Y. Chen, *Nanotechnology,* 2005, **16**, 2282-2287.

9 G. S. Painter, F. W. Averill, P. F. Becher, N. Shibata, K. Benthem, and S. J. Pennycook, *Phys. Rev. B,* 2008, **78**, 214206.

10 X. F. Lu, H. J. Wang, M. Chen, L. Fan, C. Wang and S. H. Jia, *Phys. Chem. Chem. Phys.,* 2013, **15**, 6175-6178.

Physical Chemistry Chemical Physics Accepted Manuscript

11 X. F. Lu, M. Chen, D. Qiu, L. Fan, C. Wang and H. J. Wang, *Comp. Mater. Sci.,* 2012, **62**, 17-22.
12 X. F. Lu, D. Qiu, M. Chen, L. Fan, C. Wang, H. J. Wang and G. J. Qiao, *Mater. Res. Innov.,* 2013, **17**, 201-206.
13 W. Y. Ching, P. Rulis, L. Z. Ouyang and A. Misra, *Appl. Phys. Lett.,* 2009, **94**, 051907.
14 A. Nakano, R. K. Kalia and P. Vashishta, *Phys. Rev. Lett.,* 1995, **75**, 3138-3140.
15 J. Chen, L. Z. Ouyang, P. Rulis, A. Misra and W. Y. Ching, *Phys. Rev. Lett.,* 2005, **95**, 256103.
16 M. M. Caruso, D. A. Davis, Q. Shen, S. A. Odom, N. R. Sottos, S. R. White and J. S. Moore, *Chem. Rev.,* 2009, **109**, 5755-5798.
17 M. M. Boyle, R. A. Smaldone, A. C. Whlley, M. W. Ambrogio, Y. Y. Botros and J. F. Stoddart, *Chem. Sci.,* 2011, **2**, 204-210.
18 K. Ariga, T. Mori and J. P. Hill, *Adv. Mater.,* 2012, **24**, 158-176.
19 X. F. Lu, M. Chen, L. Fan, C. Wang, H. J. Wang and G. J. Qiao, *Appl. Phys. Lett.,* 2013, **102**, 031907.
20 J. Tersoff, *Phys. Rev. B,* 1988, **38**, 9902-9903.
21 J. Tersoff, *Phys. Rev. B,* 1989, **39**, 5566-5568.
22 W. K. Chan, M. Luo and T. Y. Zhang, *Scripta Mater.,* 2008, **59**, 692-695.
23 V. Tomar, M. Gan and H. S. Kim, *J. Eur. Ceram. Soc.,* 2010, **30**, 2223-2237.
24 V. Tomar and M.Gan, *Int. J. Hydrogen Energy,* 2011, **36**, 4605-4616.

Physical Chemistry Chemical Physics Accepted Manuscript

This journal is © The Royal Society of Chemistry [year]